Nuclear Inst. and Methods in Physics Research B 462 (2020) 95–101

Contents lists available at ScienceDirect

Nuclear Inst. and Methods in Physics Research B

journal homepage: www.elsevier.com/locate/nimb

High efficiency resonance ionization of thorium☆

Y. Liu*, D.W. Stracener

Physics Division, Oak Ridge National Laboratory, Oak Ridge, TN 37831, USA

ARTICLE INFO

Keywords:
Thorium
Resonance ionization
Mass spectrometry
Ti:Sapphire laser
Ionization efficiency

ABSTRACT

Multi-step resonance ionization spectroscopy of thorium has been performed with Ti:Sapphire lasers and a hot-cavity laser ion source. Resonance ionization schemes involving three-color, three-photon ionization processes are evaluated and a new three-photon scheme is demonstrated with measured overall ionization efficiency of 38.6(5)%. This high efficiency makes it possible to determine the thorium impurities in materials used for ultra-low background neutrino detectors and could also benefit ultra-trace thorium analysis using resonance ionization mass spectrometry for various radiochemical tracer applications.

1. Introduction

Thorium (Th) isotopes are of great interest to fundamental research and applied applications. The ^{229}Th isotope is unique in nuclear physics due to its possession of an isomer state ^{229m}Th that has the lowest nuclear excitation energy known in nature – approximately 7.8 eV above the nuclear ground state ^{229g}Th [1]. This isomeric state could allow for direct laser excitation [2,3] with novel applications such as constructing a nuclear clock with unprecedented precision [4,5] and demonstrating a nuclear laser [6]. Yet, the precise knowledge of this isomer state, including its exact energy [7,8] and lifetime [9], is still waiting to be experimentally determined [10–13]. Long-lived Th-series isotopes are key radiochemical tracers for various applications, such as nuclear forensics and nonproliferation safeguards [14–16], ocean biogeochemical modeling [17–19], geochronology and archeology [20–22], stellar age-dating [23,24], and cancer therapy [25]. ^{232}Th is the dominant and only naturally-occurring isotope of thorium, with other isotopes being intermediate decay products and thus present at very low trace levels. Accordingly, highly sensitive analytical techniques are needed for detecting thorium isotopes in environmental and commercial materials [26].

Resonance ionization mass spectrometry (RIMS) is increasingly used for the analysis of trace actinide radioisotopes (U, Pu, Th) [26–31]. In RIMS, ions are formed by stepwise resonant absorption of two or three photons through allowed atomic levels to photoionization [32,33]. The multistep resonance process is extremely selective for the specific atoms of interest and can be performed very efficiently [34–36]. Hence, RIMS is superior in suppressing atomic and molecular isobaric interferences and capable of ultrahigh sensitivity comparable with or better than other mass spectrometry techniques. A crucial component for RIMS to be technically viable for ultra-trace actinide analysis is to realize the highest possible ionization efficiency and thus the lowest detection limit.

In this paper we report the development of highly efficient laser ionization schemes for thorium. The work is specifically aimed at improving the sensitivity and detection limit of RIMS for qualitative and quantitative analysis of unwanted ultra-trace actinide impurities in the materials used to fabricate ultralow-background detectors for nuclear research, such as the enriched ^{76}Ge detector for the Majorana Demonstrator neutrinoless double-beta-decay experiment [37] for which thorium and uranium impurities are expected to be the dominant sources of background and must be below the levels of a few 10^{-14} by mass. This study is also important to enhancing the production of the exotic ^{229m}Th beam using a laser ion source [38–40] and increasing the sensitivity of high-resolution spectroscopy of Th isotopes in a gas cell [39] and in a gas jet [41,42].

Thorium (Z = 90) has the atomic ground-state electronic configuration of [Rn]$6d^2 7s^2$ with a partially occupied 6*d*-shell and an empty 5*f*-shell located inside the outer 7*s*-shell. Interaction between the open subshells is expected to give rise to a large number of energetically

* Corresponding author.
E-mail address: liuy@frib.msu.edu (Y. Liu).

https://doi.org/10.1016/j.nimb.2019.11.006
Received 20 September 2019; Received in revised form 4 November 2019; Accepted 4 November 2019
Available online 14 November 2019
0168-583X/

adjacent electronic states. Complicated spectra with high density bound and autoionizing (AI) electronic states are indeed observed in laser ionization spectroscopy [38,43–46]. As a result, experimental determination of the optimal ionization scheme for Th requires systematic and time-consuming evaluation of the spectra. Two- [43–46] and three-step [38] resonance ionization of Th has been studied. An extensive spectroscopy investigation was recently performed by Raeder et al. [38,47] using Ti:Sapphire lasers at Mainz University, who observed many new bound and AI levels in Th and suggested a number of ionization schemes involving three resonant steps. However, for this earlier work, the best overall laser ionization efficiency was 0.6% [38].

In a previous study [48], we evaluated one of the three-step schemes developed at Mainz and obtained an overall ionization efficiency of about 32% using a hot-cavity resonance ionization laser ion source (RILIS). For the present study, we have conducted spectroscopy surveys of the high-lying and AI levels in Th, in order to identify more suitable three-step ionization pathways, and systematically evaluated the relative efficiencies of different three-step schemes under similar experimental conditions. A more efficient scheme is demonstrated with an overall ionization efficiency of near 40%. The experimental procedure and results are described.

2. Experimental

The ionization scheme studied in this work, involving three resonant steps, is presented in Fig. 1. Spectroscopic surveys are conducted with a set of three tunable Ti:Sapphire lasers. The thorium atom is excited from the ground state $6d^27s^2\ ^3F_2$ to the first excited state $6d^27s7p\ ^3G_3^o$ at 26878.16 cm^{-1} [49] by a frequency-doubled photon of λ_1 = 372.049 nm from one of the Ti:Sapphire lasers. This first transition is known, selected by Raeder et al. [38] and used in our previous work [48]. A second photon (λ_2) then excites the atom to an intermediate resonant state (E_2) from which it is ionized by a third photon (λ_3). The second and third step photons are provided by the other two Ti:Sapphire lasers. The wavelength of the second laser (λ_2) is scanned to search for E_2 resonance transitions and then, with λ_2 fixed to a selected E_2 level, the third laser wavelength (λ_3) is scanned to look for strong resonant photoionization signals via high-lying Rydberg or AI states.

The laser system [48,51] consisted of three grating-tuned

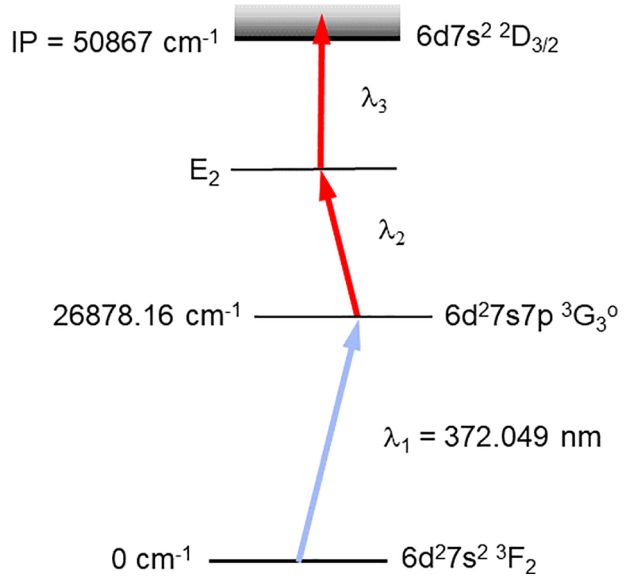

Fig. 1. Three-step resonance ionization scheme for Th, with values of the energies and ionization potential (IP) from Refs. [38,50]. The second (λ_2) and third (λ_3) laser wavelengths are scanned separately to search for overall strong ionization resonances.

Ti:Sapphire lasers continuously tunable between 720 nm and 960 nm with maximum output power of about 2.5 W near 810 nm. One of the laser outputs was frequency-doubled to provide the first resonant excitation at 372.049 nm. The frequency-doubled laser output was available in wavelengths of 360–470 nm with maximum power of about 800 mW at 405 nm. The spectral linewidths of the lasers were on the order of 3–4 GHz for the fundamental light and 4–5 GHz for frequency-doubled light. The three Ti:Sapphire lasers were individually pumped by three Q-switched Nd:YAG lasers at 532 nm at a pulse repetition rate of 10 kHz, so the Ti:Sapphire lasers were pulsed at 10 kHz with pulse widths of about 30 ns. The three lasers were synchronized by adjusting the external trigger timing to the individual pump lasers. The time jitter between the synchronized lasers was typically not > 5 ns, which was small in comparison with the laser pulse width. Intentionally desynchronizing the laser pulses up to 10 ns with respect to each other had little effect on the ion signal intensity.

The study was conducted with RILIS and the mass separator at the Injector for Radioactive Ion Species 2 (IRIS2) platform at Oak Ridge National Laboratory (ORNL). Details of the experimental setup have been described elsewhere [51]. In brief, a hot-cavity ion source was mounted on the IRIS2 platform, As illustrated in Fig. 2, the ion source consisted of Ta tubular cavity (ϕ3 × 30 mm) and a Ta sample-tube (ϕ8.5 × 100 mm). The ion source was resistively heated by an electrical current. Thorium sample materials were heated and evaporated inside the sample tube and the volatile species effused into the cavity where they were selectively ionized by laser beams from the Ti:Sapphire lasers. The ions were extracted from the cavity, accelerated to 40 keV, and transported to a magnetic mass separator with mass resolving power of 1000 for mass number A = 100. The mass separator was optimized for transmission of an A = 232 ion beam and the ^{232}Th ion beam intensity passing through the mass separator was measured with a Faraday cup (FC). The total ion beam intensity before the mass separator was periodically monitored with a retractable FC. The laser beams were collimated and sent into the IRIS2 beamline through a vacuum window, traveling in the opposite direction of the ion beam and entering the 3-mm cavity of the ion source through the ion extraction electrode. The laser beams were focused to a waist on the order of 3-mm in diameter at the ion source. The laser power injected into the cavity was about 100 mW of frequency-doubled light and 1 W of the fundamental light. The corresponding laser power density in the laser-atom interaction region was about 1.5 W/cm^2 for the first-step transition and 15 W/cm^2 for the second and third transitions.

Photoionization spectra were obtained by recording the ion current measured at the FC after the mass separator as a function of the laser wavelength. The laser wavelength could be scanned in the direction of increasing photon energy (scan-up) or decreasing photon energy (scan-down). We observed that the spectral line centroids obtained from the scan-up and scan-down measurements were slightly different with an average difference of about 0.04 cm^{-1}. Thus, each spectrum was measured at least twice by scan-up and scan-down, respectively, to account for the hysteresis in laser scans. The line centroids were then determined as the average values of the scan-up and scan-down measurements. The fundamental wavelengths of the three lasers were monitored simultaneously using a calibrated wavelength meter (HighFinesse WS6-600) equipped with a 4-channel opto-mechanical switcher. The systematic uncertainty in measuring the laser wavelengths was dominated by the absolute accuracy of the wavelength meter, which was 600 MHz or 0.02 cm^{-1} according to a 3-sigma criterion.

The Th samples were made from 1000 ppm Th atomic absorption (AA) standard solutions with Th in a nitric acid matrix in the form of thorium nitrate. Typical sample sizes were 20 μg or 40 μg of Th, corresponding to about 5 × 10^{16} and 10^{17} Th atoms per sample, respectively. A sample was prepared with 20 or 40 μL AA solution dried on a thin Ti metal foil (0.0005-inch thick and about 5 × 6 mm in size) and wrapped in the foil. The Ti foil was used as the reducing agent to release

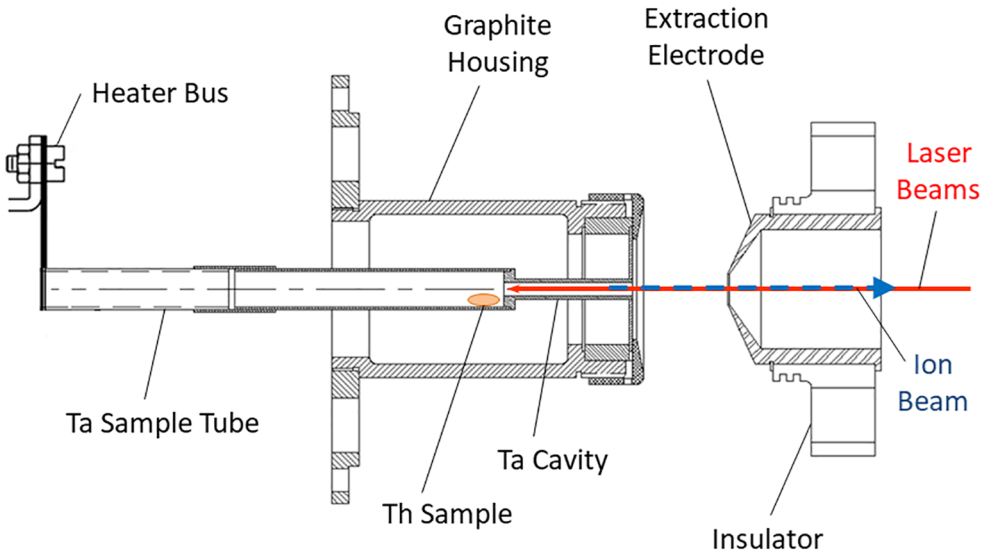

Fig. 2. Schematic of the hot-cavity ion source assembly and laser ionization configuration.

the bound Th atoms from the sample matrix. The sample was heated in the sample-tube of the ion source assembly to provide atomic Th for measurement. We have previously observed [52] that oxides, e.g., ThO, were released from the nitrate sample at relatively low temperatures and dissociated into the atomic components at high temperatures. The sample tube was colder than the cavity and the temperature along the sample tube decreased with the distance away from the cavity. Therefore, the Th sample was placed very close to the cavity, as shown in Fig. 2, in order to reach the high temperatures required for significant decomposition of ThO into atomic Th. For the spectroscopy measurements reported here, the ion source was heated with a current of up to 380 A where the Th sample temperature was estimated to be around 1950 K and the cavity was on the order of 2100 K. Thorium ion currents measured at the FC after the mass-separator were on the order of 10 nA for strong peaks. Under this heating condition, a 40 μg sample lasted for more than three days.

3. Results

3.1. Second excited states

Fig. 3 shows the ionization spectra for the second laser λ_2 scanned over the range of 777–872 nm or 11468–12870 cm^{-1}. The peaks correspond to resonant excitations of Th to intermediate excited states from the $6d^27s7p\ ^3G_3^o$ state at 26878.16 cm^{-1}. The plot shows the spectrum obtained with the third laser (λ_3) arbitrarily set to a photon energy of 13062.7 cm^{-1}, high enough to ionize the Th atoms from the intermediate levels populated in the λ_2 scan. We also measured a portion of the spectrum with the third laser blocked. In this case, the excited atoms were ionized by absorbing another photon from the first or second lasers. In this case, the spectral lines were typically much smaller than those with the third laser on, due to lower ionization probabilities without the third laser, but the line positions obtained in both cases were in excellent agreement, as shown in Fig. 4. A total of 23 resonance lines were observed, corresponding to intermediate excited states of even parity with level energies given by $E_2 = E_1 + h\nu_2$, where E_1 = 26878.16 cm^{-1}, h is Planck's constant, and ν_2 is the second laser frequency at the line centers determined by Gaussian fits. Table 1 lists the measured energies E_2 for the levels observed in Fig. 3, along with the literature values. The scans were performed with coarse resolutions of about 3 GHz per scan step. As a result, the statistical error of the line positions was on the order of 0.15 cm^{-1}. Nevertheless, we could confirm all the 23 states with reasonable agreement with literature.

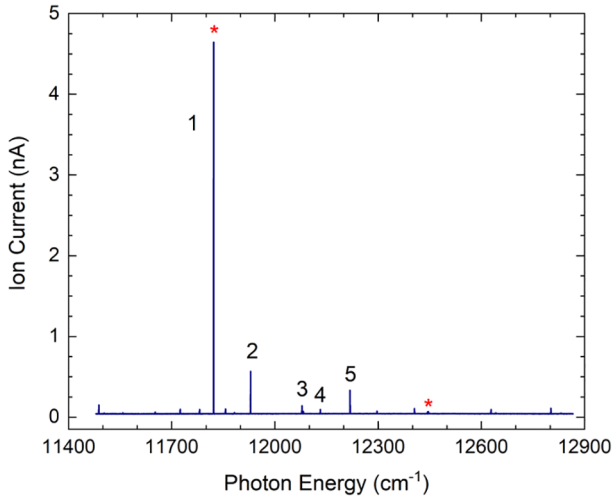

Fig. 3. Photoionization spectra obtained by scanning the second laser wavelength (λ_2) with the third laser (λ_3) set at wavenumber of 13062.7 cm^{-1}. Lines labeled 1–5 are selected as the second excited state (SES) in this work; and the lines marked with the symbol, *, are the SES used by Raeder et al. [38].

Five E_2 levels, labeled 1–5 in Fig. 3, were selected as the second excited states (SES) for three-step resonance ionization based on their relative line intensities in the λ_2 scan with the third laser on. Table 2 gives more information for these selected transitions. From the E_1 = 26878.16 cm^{-1} level, Raeder et al. [38] selected three SES at 38700.25, 39321.81, and 39997.59 cm^{-1}, respectively. The first is the strongest peak (#1) used in this work, the second turned out to be a very weak line in our spectrum as marked by * in Fig. 3, and the third is out of our λ_2 scan range.

3.2. Three-step resonant ionization

Fig. 5 shows the three-photon and three-color photoionization spectra from the selected SES, measured by scanning the third laser wavelength (λ_3) while the first and second laser were fixed to the respective resonant transitions. The λ_3 scans covered the range 50500–52100 cm^{-1} in total excitation energy, revealing high density of states and complex spectra below and above the ionization potential (IP) of Th. We have identified Rydberg series converging to the IP in some of the spectra, but no AI Rydberg series were observed. Analysis of

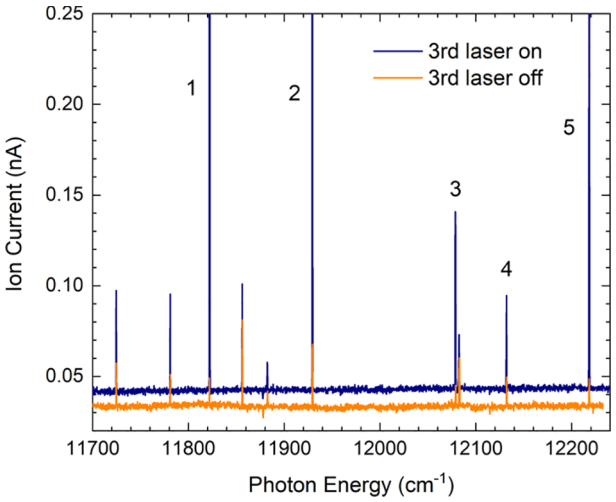

Fig. 4. Comparison of the λ_2 scan spectra obtained with the third laser on and off. Lines labeled 1–5 are selected second excited states for three-step ionization in this work. For clarity, the spectrum with the 3rd laser off is moved down by an artificial offset of -0.01 nA.

Table 1
Measured energies of the intermediate excited states observed in λ_2 scans. The uncertainty is the standard deviation of the scan-up and scan-down measurements, not including the systematic error of 0.02 cm^{-1}. Columns 2 and 3 are the energy and J value, respectively, in literature [50], and Column 4 is the energy measured by Raeder et al. [38].

E_2 (cm^{-1}) this work	E_2 (cm^{-1}) from Ref. [50]	J from Ref. [50]	E_2 (cm^{-1}) from Ref. [38]
38366.47(3)	38366.5775	4	
38382.07(15)	38382.148	3	
38436.32(15)	38436.4152	2	
38443.74(15)	38443.8055	3	38443.82(6)
38529.81(18)	38529.929	3	
38602.95(2)	38602.9891	2	
38659.24(3)	38659.2178	2	
38700.28(3)	38700.2507	4	
38734.40(15)	38734.4088	3	
38760.63(17)	38760.6326	4	
38807.60(6)	38807.6687	2	
38956.93(20)	38956.8948	4	
38960.70(23)	38960.6542	2	38960.68(7)
39010.18(14)	39010.1797	3	
39096.36(15)	39096.2986	4	
39175.09(15)	39174.9152	3	
39283.99(15)	39283.8257	4	
39321.94(15)	39321.8086	3	
39324.41(15)			39324.25(7)
39506.57(15)	39506.39	3	
39520.46(15)	39520.19	4	
39680.60(15)	39680.4585	2	
39710.17(15)			39710.05(6)

Table 2
Selected SES and corresponding laser excitation wavelength for the second-step transition. The level energies and J values are the literature values [50].

Peak	E_2 (cm^{-1})	J	λ_2 (nm)
1	38700.2507	4	845.87
2	38807.6687	2	838.26
3	38956.8948	4	827.90
4	39010.1797	3	824.27
5	39096.2986	4	818.46

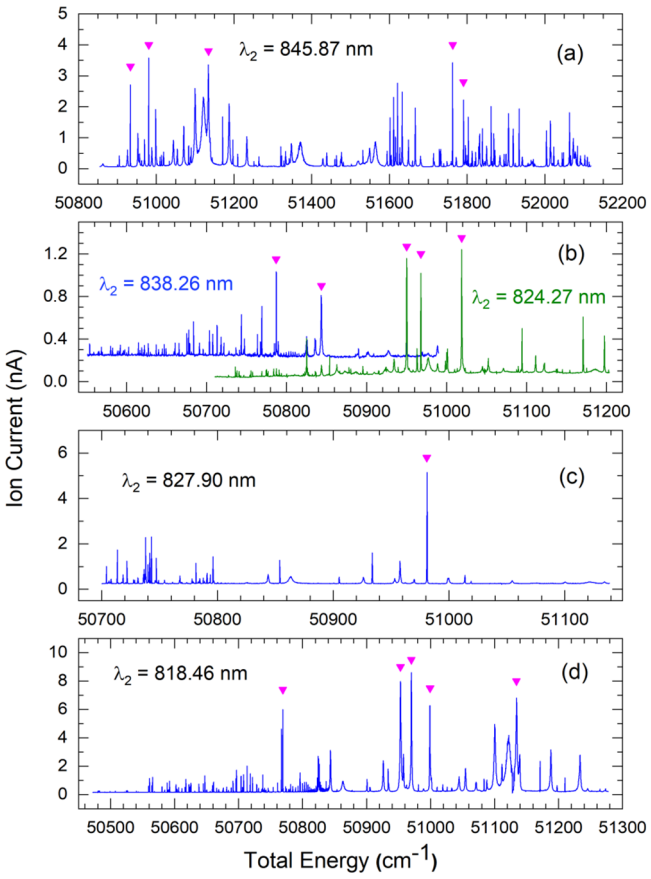

Fig. 5. Photoionization spectra excited from selected SES in Table 2, obtained by scanning the third laser wavelength λ_3. Spectral peaks marked by (▽) are selected for further evaluation. Note the differences in the ion intensity (vertical) scale and the slight differences in the scanned energy scale.

the Rydberg series is in progress and will be reported in a forthcoming publication.

It can be seen in Fig. 5 that the spectral peak intensities from different SESs differ significantly. The differences could be related to the overall ionization efficiency and could also be affected by experimental parameters since the measurements were conducted at different times and under different source operation conditions. It was therefore necessary to compare the ionization schemes under similar experimental conditions while the lasers were optimized for the respective schemes. Hence, we selected the strongest resonances from each SES for further evaluation. Sixteen resonances were chosen as indicated in Fig. 5 and the corresponding second and third excitations, centroid energy of the resonances, and possible J values are detailed in Table 3. The first excitation was the same for all the schemes (Fig. 1). Three of the resonance energies were below the IP. The J values were determined by comparing the spectra from SESs of different J.

The further evaluation was performed as follows. The ion source was maintained at a heating current of 380 A. The second and third lasers were tuned to an ionization scheme, optimized in wavelength and power, and the intensity of ^{232}Th ions was recorded. Then, the lasers were quickly tuned to another scheme, optimized, and the corresponding ion current was measured. Changing between ionization schemes typically took 10–20 min, including optimization of the laser tuning and the beamline optics for ion extraction and transportation. The relatively short switching time allowed consecutive schemes to be evaluated under similar experimental conditions. In addition, the ion current of a reference scheme was measured periodically for calibration of the slow drifts in ion current due to consumption of the Th sample or

Table 3
Comparison of the strongest resonances of odd parity from selected SES with relative ion intensity normalized to the reference scheme shown in bold. E_3 is the total excitation energy. The first excitation was the same for all the schemes (Fig. 1).

E_2 (cm^{-1})	λ_2 (nm)	E_3 (cm^{-1})	J	λ_3 (cm^{-1})	Rel. Int.
38700.2507	845.87	50933.51(21)	3, 4, 5	817.44	0.8
38700.2507	845.87	50980.93(25)	3, 4, 5	814.29	1.0
38700.2507	845.87	51134.33(23)	3, 4, 5	804.24	1.0
38700.2507	**845.87**	**51762.95(21)**	**3, 4, 5**	**765.54**	**1**
38700.2507	845.87	51790.73(15)	3, 4	763.91	1.1
38807.6687	838.26	50787.08(15)	2, 3	834.77	0.05
38807.6687	838.26	50843.53(9)	3	830.85	0.04
38956.8948	827.90	50980.98(5)	3, 4, 5	831.66	1.23
39010.1797	824.27	50950.21(15)	2, 3	837.52	0.16
39010.1797	824.27	50967.93(15)	2, 3, 4	836.28	0.14
39010.1797	824.27	51018.93(15)	3, 4	832.73	0.17
39096.2986	818.46	50769.09(9)	3	856.69	0.3
39096.2986	818.46	50953.00(8)	3, 4, 5	843.40	0.4
39096.2986	818.46	50969.95(12)	3, 4, 5	842.20	0.4
39096.2986	818.46	50998.91(15)	3, 4, 5	840.15	0.3
39096.2986	818.46	51134.27(10)	3, 4, 5	830.70	0.3

variations in the ion source condition and the beamline tuning. The reference scheme was the scheme used in our previous work [48] with λ_2 = 845.87 nm (SES at 38700.2507 cm^{-1}) and λ_3 = 765.54 nm to the AI state of total energy E_3 = 51762.95(21) cm^{-1}. It was one of the strongest AI resonances in this search. Finally, the measured ion intensities from the evaluated schemes were normalized to that of the reference scheme and the resulting relative intensities are given in Table 3.

The best scheme identified, which gave the largest relative ion intensity, was the third transition to the AI state of odd parity at 50980.98(5) cm^{-1} (λ_3 = 831.66 nm) from E_2 = 38956.8948 cm^{-1} (λ_2 = 827.90 nm). Besides the best scheme, the five AI resonances starting from E_2 = 38700.2507 cm^{-1} showed much higher ion intensities than those from other SESs. This is consistent with the results of Raeder et al. [38], who observed the strongest AI peaks from E_2 = 38700.2507 cm^{-1} and selected the AI transition to E_3 = 51762.95(21) cm^{-1} as the best scheme – the reference scheme in Table 3.

It is noteworthy to mention that for the best scheme, the second-step excitation was not the strongest but a rather weak resonance (peak #3) in the λ_2 scan (Figs. 3 and 4). We have observed similar results in the studies of laser ionization schemes for uranium and plutonium. This indicates that the peak intensity in the λ_2 scan may not be the best criteria for SES selection for these elements, because the λ_2 spectrum could be affected by coincidences where the third photon was accidentally on or near a resonance transition to an AI state. It also suggests that a more suitable SES could possibly be found among the other E_2 levels not selected here.

The selectivity of the three-step scheme was checked by blocking the individual lasers and the results showed that approximately 98.8% of the laser ionized ions were produced by three-step, three-photon ionization, about 1% were ionized by λ_1 photons alone and 0.2% by $\lambda_2 + \lambda_3$ photons.

3.3. Ionization efficiency

We measured the overall ionization efficiency of the newly identified scheme that gave the largest relative ion intensity in this study: $7s^2\ ^3F_2 \rightarrow 7s7p\ ^3G^o_3 \rightarrow 38956.8948\ \text{cm}^{-1} \rightarrow 50980.98\ \text{cm}^{-1}$ with excitation wavelengths of λ_1 = 372.049 nm, λ_2 = 827.90 nm, and λ_3 = 831.66 nm. The efficiency was determined using a calibrated sample made from 20 μL of the Th AA solution dried on a thin Ti foil, as described above in Section 2. The sample contained a total of 5.19(7) × 10^{16} Th atoms, with uncertainty given by the uncertainty of the certified Th AA solution concentration and the accuracy of the pipette used to prepare the sample. Fig. 6 shows the efficiency measurement process as well as the result. With the three Ti:Sapphire lasers tuned and optimized to the respective excitations, we heated the ion source to high temperatures by gradually increasing the electrical heating current and simultaneously recording the mass-selected ^{232}Th ion beam intensity. The laser power used in the measurement was about 150 mW, 1.5 W, and 1.5 W for the first, second, and third excitations, respectively. ^{232}Th ions of about 2 pA were measured at source heating current of 275 A. Data recording started when the observed ^{232}Th ion current reached 0.1nA at a heating current of 300 A. The heating current was increased in 10 A steps up to 410 A in about 3.5 h. At the maximum heating current, the cavity temperature was on the order of 2200 K. The ^{232}Th ion intensity increased to about 50 nA and then decreased very slowly. The measurement was stopped after about 28.5 h when the ion intensity dropped to less than 20 nA, due to time constraints and the consideration that further accumulation of eight more hours would only contribute about 2% to the overall efficiency based on the downward slope of the ion intensity. The ionization efficiency was then determined as the ratio of the total number of ions detected to the total number of neutral atoms in the sample. From the data in Fig. 6, an overall efficiency of 38.6(5)% was obtained. A smooth extrapolation of the ion intensity for the next 6.5 h indicates that the overall efficiency could be as high as 40%.

Thorium could also be surface ionized in the Ta hot-cavity. During the measurement the ^{232}Th ion intensity due to surface ionization was frequently checked by blocking all the laser beams – the ion intensity measured at the FC without the lasers was from surface ionization. As shown in Fig. 6, the vertical lines correspond to lasers being blocked. The maximum surface ion intensity observed was only about 70 pA. Consequently, the surface ionization contribution can be ignored. It is also seen in Fig. 6 that the measured ion intensity for two periods between t = 13–16 h was zero, due to high-voltage interlock faults that occurred at t = 13–15 h and again at t = 15.3–15.7 h, during which data transfer from the FC was interrupted. We used linear interpolation to include the missing data.

The ionization efficiency of the reference scheme was previously measured as 31.5% [48]. The ratio of the efficiency measured here for the new scheme to that of the reference scheme is 38.6/31.5 = 1.22 or 40/31.5 = 1.27, in agreement with the relative ion intensity of the two schemes as shown in Table 3.

4. Discussion

An objective of this study is to detect ultra-trace amounts of Th impurity in the copper materials used in the construction of detectors for neutrinoless double-beta-decay experiments. In order to reduce the background from Th to acceptable levels in these experiments, the mass ratio of Th to Cu needs to be below 75 fg ^{232}Th/g Cu [37]. This corresponds to about 2 × 10^5 ^{232}Th atoms per mg Cu. The Th sample sizes used in this study were 20–40 μg of ^{232}Th. Using sample sizes of 4 × 10^4–10^9 Pu atoms, and an overall resonance ionization efficiency of 0.5 − 5%, Raeder et al. [28] reported a detection limit of 10^4–10^5 Pu atoms by in-source RIMS using a hot-cavity RILIS similar to the one used in the present study. Based on their results and the high ionization efficiency for Th demonstrated here, the Th sample amount could potentially be scaled down to sub-femtogram levels and the overall detection limit could be down to less than 10^4 Th atoms. Thus, our RIMS setup with the FC replaced by a detector sensitive for single ion detection, such as a microchannel plate or a channeltron detector, is very promising to enable qualitative and quantitative analysis of trace Th amounts in copper materials at or below the level of 2 × 10^5 Th atoms per milligram Cu.

To our knowledge, the measured ionization efficiency of 38.6(5)% is the highest efficiency for thorium to date. We believe that more efficient ionization schemes are still possible since the possible

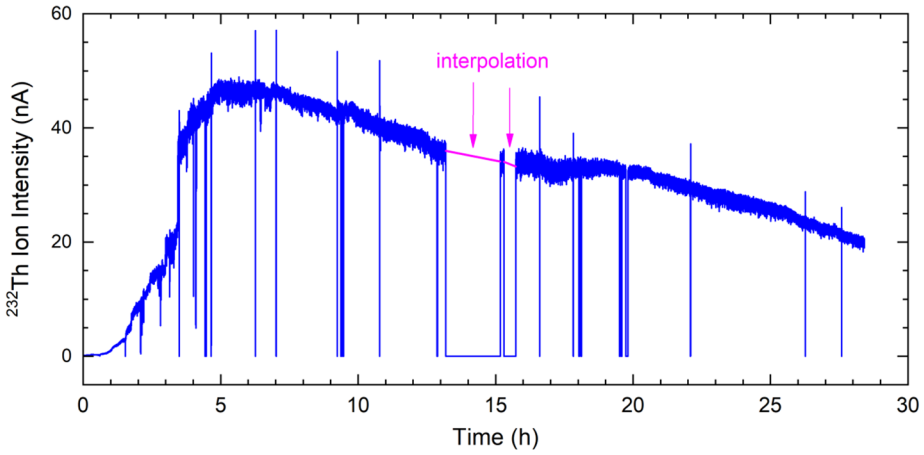

Fig. 6. Measured ^{232}Th ion beam intensity during the efficiency measurement. The vertical lines down to the baseline correspond to lasers being blocked. The communication with the FC was interrupted by two interlock faults between t = 13 and 16 h. The missing data for these two periods are assumed using a smooth interpolation.

combinations of the excitation and ionization transitions for Th are by no means exhausted. The following approaches can be considered for future investigation. First, many of the AI resonances previously reported [38,44] are above the energy range of this study and have not been evaluated. Second, only five SES were evaluated based on their relatively strong line intensities in the λ_2 scan. Since we have observed that a weak line in the λ_2 scan can lead to a highly efficient final ionization, other E_2 levels should be investigated for more efficient three-step schemes. Third, this study was limited to one first-step transition. A future improvement could be to implement an autotracking frequency-doubling system for our Ti:Sapphire lasers, which provides automatic phase matching optimization as the input fundamental wavelength is changed and allows continuous λ_1 scan to search for more suitable first-step excitations. In addition, we can also investigate simpler two-step resonance ionization schemes that use frequency-doubled photons for both steps. Very recently, highly efficient two-step resonance ionization schemes have been demonstrated for lanthanides [36]. Thorium release and atomization during sample vaporization could still be a limiting factor for the overall efficiency. This process strongly depends on the source temperature, the chemical properties of the sample, the reducing agent, and the ion source materials. In previous work on surface ionization, we have evaluated different metal foils, Ti, Zr, and Ta, as the reducing agent for the release of U from the nitric acid matrix. Using a Ta-cavity source, we observed that the overall ionization efficiency for U was improved from 0.9% (Ti foil) to 1.4% (Zr foil) and 2.5% (Ta foil) and the U^+/UO^+ intensity ratio also improved significantly from Ti to Ta foils. Since uranium oxides have very high melting points, one of the reasons for the improvements could be the higher melting points of Zr and Ta to better match with the thermochemical property of the sample. Based on this, we expect Zr or Ta foils to be a better reducing agent for Th as well. In fact, Raeder et al. used Zr foil for both U [53] and Th [38]. Therefore, it may be possible to further improve the overall ionization efficiency by using a different reducing metal, such as Zr and Ta.

We previously studied surface ionization of U and Th [52] with a hot-cavity surface ionization source, which is the same hot-cavity ion source used in this study without lasers. In the case of surface ionization, molecular ions of UO^+ and ThO^+ were always observed first and were the dominant ions as the ion source was heated up. The atomic U^+ and Th^+ ions were typically observed at very high heating currents of 450 A and above (T > 2300 K in the cavity). Since Th has a lower IP (6.31 eV) as compared to that of ThO (6.6 eV) and thus a higher surface ionization probability than ThO, these observations indicated that the oxides were released from the nitrate samples and they dissociated into the atomic components at high temperatures (> 2300 K). In contrast, the operating temperature for laser ionization was significantly lower. In this work, laser ionized atomic Th^+ ions were observed at heating currents as low as 270 A (T ~ 1700 K) and all the laser spectroscopy measurements were conducted at a heating current of 380 A (T ~ 2100 K). A hypothesis is laser-induced breakup of the thorium oxides inside the ion source.

5. Conclusion

Spectroscopic surveys of Th have been performed using Ti:Sapphire lasers and a hot-cavity RILIS to search for more efficient three-step resonance ionization schemes. For the second step, 23 intermediate excited states were observed and confirmed with the literature. Photoionization spectra from five of the intermediate states were measured and sixteen of the strongest resonance ionization transitions were further evaluated under similar ion source operating conditions. An improved three-step scheme has been identified with an overall ionization efficiency measured to be 38.6(5)%. This high efficiency makes it possible to detect Th impurities in materials used for ultra-low background neutrino detectors and, in general, could improve RIMS analysis of ultra-trace Th isotopes for various applications. It could also enable the production of thorium isotope beams, including the predicted lowest-energy exotic nuclear isomer ^{229m}Th, for forefront nuclear physics studies.

CRediT authorship contribution statement

Y. Liu: Conceptualization, Investigation, Formal analysis, Writing - original draft. **D.W. Stracener:** Investigation, Project administration, Writing - review & editing.

Declaration of Competing Interest

The authors declare that they have no known competing financial interests or personal relationships that could have appeared to influence the work reported in this paper.

Acknowledgements

This material is based upon work supported by the U.S. Department of Energy, Office of Science, Office of Nuclear Physics and this research used resources of the Holifield Radioactive Ion Beam Facility of Oak Ridge National Laboratory, which was a DOE Office of Science User Facility.

References

[1] B.R. Beck, C.Y. Wu, P. Beiersdorfer, G.V. Brown, J.A. Becker, K.J. Moody, J.B. Wilhelmy, F.S. Porter, C.A. Kilbourne, R.L. Kelley, Improved value for the energy splitting of the ground-State doublet in the Nucleus 229mTh, Report No. LLNL-PROC-415170, 2009.

[2] L. von der Wense, B. Seiferle, S. Stellmer, J. Weitenberg, G. Kazakov, A. Pálffy,

P.G. Thirolf, A laser excitation scheme for ^{229m}Th, Phys. Rev. Lett. 119 (2017) 132503.
[3] S. Stellmer, G. Kazakov, M. Schreitl, H. Kaser, M. Kolbe, T. Schumm, Attempt to optically excite the nuclear isomer in ^{229}Th, Phys. Rev. A 97 (2018) 062506.
[4] C.J. Campbell, A.G. Radnaev, A. Kuzmich, V.A. Dzuba, V.V. Flambaum, A. Derevianko, Single-ion nuclear clock for metrology at the 19th decimal place, Phys. Rev. Lett. 108 (2012) 120802.
[5] F.F. Karpeshin, M.B. Trzhaskovskaya, The ^{229}Th isomer line as a reference for a high-precision frequency standard, Meas. Tech. 59 (2016) 722.
[6] E.V. Tkalya, Proposal for a nuclear gamma-ray laser of optical range, Phys. Rev. Lett. 106 (2011) 162501.
[7] J. Jeet, C. Schneider, S.T. Sullivan, W.G. Rellergert, S. Mirzadeh, A. Cassanho, H.P. Jenssen, E.V. Tkalya, E.R. Hudson, Results of a direct search using synchrotron radiation for the low-energy ^{229}Th nuclear isomeric transition, Phys. Rev. Lett. 114 (2015) 253001.
[8] L. von der Wense, B. Seiferle, M. Laatiaoui, J.B. Neumayr, H.-J. Maier, H.-F. Wirth, C. Mokry, J. Runke, K. Eberhardt, C.E. Düllmann, N.G. Trautmann, P.G. Thirolf, Direct detection of the ^{229}Th nuclear clock transition, Nature 533 (2016) 47.
[9] N. Minkov, A. Pálffy, Reduced transition probabilities for the gamma decay of the 7.8 eV isomer in ^{229}Th, Phys. Rev. Lett. 118 (2017) 212501.
[10] J. Thielking, M.V. Okhapkin, P. Głowacki, D.M. Meier, L. von der Wense, B. Seiferle, C.E. Düllmann, P.G. Thirolf, E. Peik, Laser spectroscopic characterization of the nuclear-clock isomer ^{229m}Th, Nature 556 (2018) 321.
[11] L.C. von der Wense, B. Seiferle, C. Schneider, J. Jeet, I. Amersdorffer, N. Arlt, F. Zacherl, R. Haas, D. Renisch, P. Mosel, P. Mosel, M. Kovacev, U. Morgner, C.E. Düllmann, E.R. Hudson, P.G. Thirolf, The concept of laser-based conversion electron Mössbauer spectroscopy for a precise energy determination of ^{229m}Th, Hyperfine Interact. 240 (2019) 23.
[12] T. Masuda, A. Yoshimi, A. Fujieda, et al., X-ray pumping of the ^{229}Th nuclear clock isomer, Nature 573 (2019) 238.
[13] I. Pohjalainen, I.D. Moore, T. Sajavaara, Characterization of 233U alpha recoil sources for 229(m)Th beam production, Nucl. Instrum. Methods B (2019), in press.
[14] F.E. Stanley, A beginner's guide to uranium chronometry in nuclear forensics and safeguards, J. Anal. At. Spectrom. 27 (2012) 1821–1830.
[15] K.J. Moody, P.M. Grant, Nuclear forensic analysis of thorium, J. Radioanal. Nucl. Chem. 241 (1999) 157–167.
[16] Z. Karpa, Analytical Chemistry of Uranium: Environmental, Forensic, Nuclear, and Toxicological Applications, first Edition, CRC Press, Boca Raton, FL, 2014.
[17] R.F. Anderson, Chemical tracers of particle transport, in: Henry Elderfield (Ed.), Treatise on Geochemistry, Vol. 6 Elsevier, Amsterdam, 2003, pp. 247–273.
[18] L. Coppola, M. Roy-Barman, S. Mulsow, P. Povinec, C. Jeandel, Thorium isotopes as tracers of particles dynamics and deep water circulation in the Indian sector of the Southern Ocean (ANTARES IV), Mar. Chem. 100 (2006) 299–313.
[19] C.T. Hayes, J. Rosen, D. McGee, E.A. Boyle, Thorium distributions in high- and low-dust regions and the significance for iron supply, Global Biogeochem. Cycles 31 (2017) 328–347.
[20] K.W.W. Sims, S. Pichat, M.K. Reagan, P.R. Kyle, H. Dulaiova, et al., On the time scales of magma genesis, melt evolution, crystal growth rates and magma degassing in the erebus volcano magmatic system using the ^{238}U, ^{235}U and ^{232}Th decay series, J. Petrol. 54 (2013) 235–271.
[21] M. García-Diez, D.L. Hoffmann, J. Zilhão, C. de las Heras, J.A. Lasheras, R. Montes, A.W.G. Pike, Uranium series dating reveals a long sequence of rock art at Altamira Cave (Santillana del Mar, Cantabria), J. Archaeol. Sci. 40 (2013) 4098–4106.
[22] A.W.G. Pike, D.L. Hoffmann, P.B. Pettitt, M. García-Diez, J. Zilhão, Dating palaeolithic cave art: why U-Th is the way to go, Quat. Int. 432 (2017) 41–49.
[23] R. Cayrel, V. Hill, T.C. Beers, B. Barbuy, M. Spite, F. Spite, B. Plez, J. Andersen, P. Bonifacio, P. Francois, P. Molaro, B. Nordström, F. Primas, Measurement of stellar age from uranium decay, Nature 409 (2001) 691.
[24] I.V. Panov, Yu.S. Lutostansky, M. Eichler, F.-K. Thielemann, Determination of the galaxy age by the method of uranium–thorium–plutonium isotopic ratios, Phys. Atomic Nucl. 80 (2017) 657–665.
[25] A. Morgenstern, C. Apostolidis, C. Kratochwil, M. Sathekge, L. Krolicki, F. Bruchertseifer, An overview of targeted alpha therapy with ^{225}Actinium and ^{213}Bismuth, Curr. Radiopharm. 11 (2018) 200–208.
[26] X. Hou, P. Roos, Critical comparison of radiometric and mass spectrometric methods for the determination of radionuclides in environmental, biological and nuclear waste samples, Anal. Chim. Acta 608 (2008) 105–139.
[27] N. Trautmann, G. Passler, K.D.A. Wendt, Ultratrace analysis and isotope ratio measurements of long-lived radioisotopes by resonance ionization mass spectrometry (RIMS), Anal. Bioanal. Chem. 378 (2004) 348–355.
[28] S. Raeder, A. Hakimi, N. Stöbener, N. Trautmann, K. Wendt, Detection of plutonium isotopes at lowest quantities using in-source resonance ionization mass spectrometry, Anal. Bioanal. Chem. 404 (2012) 2163–2172.
[29] S.K. Aggarwal, A review on the mass spectrometric analysis of thorium, Radiochim. Acta 104 (2016) 445–455.
[30] M.R. Savina, B.H. Isselhardt, A. Kucher, R. Trappitsch, B.V. King, D. Ruddle, R. Gopal, I. Hutcheon, High useful yield and isotopic analysis of uranium by resonance ionization mass spectrometry, Anal. Chem. 89 (2017) 6224–6231.
[31] M. Franzmann, H. Bosco, L. Hamann, C. Walther, K. Wendt, Resonant laser–SNMS for spatially resolved and element selective ultra-trace analysis of radionuclides, J. Anal. At. Spectrom. 33 (2018) 730–737.
[32] G.S. Hurst, M.G. Payne, Principles and Applications of Resonance Ionisation Spectroscopy, Adam Hilger, Bristol, Philadelphia, 1988.
[33] M.G. Payne, L. Deng, N. Thonnard, Applications of resonance ionization mass spectrometry, Rev. Sci. Instrum. 65 (1994) 2433–2459.
[34] T. Kron, Y. Liu, S. Richter, F. Schneider, K. Wendt, High efficiency resonance ionization of palladium with Ti:sapphire lasers, J. Phys. B: At. Mol. Opt. Phys. 49 (2016) 185003.
[35] F. Schneider, K. Chrysalidis, H. Dorrer, Ch.E. Düllmann, K. Eberhardt, R. Haas, T. Kieck, C. Mokry, P. Naubereit, S. Schmidt, K. Wendt, Resonance ionization of holmium for ion implantation in microcalorimeters, Nucl. Instrum. Methods B 376 (2016) 388–392.
[36] V.M. Gadelshin, R. Heinke, T. Kieck, T. Kron, P. Naubereit, F. Rösch, T. Stora, D. Studer, K. Wendt, Measurement of the laser resonance ionization efficiency for lutetium, Radiochim. Acta 107 (2019) 653–661.
[37] N. Abgrall, E. Aguayo, F.T. Avignone III, A.S. Barabash, F.E. Bertrand, et al., The MAJORANA DEMONSTRATOR neutrinoless double-beta decay experiment, Adv. High Energy Phys. 2014 (2014).
[38] S. Raeder, V. Sonnenschein, T. Gottwald, I.D. Moore, M. Reponen, S. Rothe, N. Trautmann, K. Wendt, Resonance ionization spectroscopy of thorium isotopes–towards a laser spectroscopic identification of the low-lying 7.6 eV isomer of ^{229}Th, J. Phys. B: At. Mol. Opt. Phys. 44 (2011) 165005.
[39] V. Sonnenschein, I.D. Moore, S. Raeder, A. Hakimi, A. Popov, K. Wendt, The search for the existence of ^{229m}Th at IGISOL, Eur. Phys. J. A 48 (2012) 52.
[40] I. Pohjalainen, Gas-Phase Chemistry, Recoil Source Characterization and in-gas-cell Resonance Laser Ionization of Actinides at IGISOL, Ph.D. thesis University of Jyväskylä, 2018.
[41] Yu. Kudryavtsev, R. Ferrer, M. Huyse, P. Van den Bergh, P. Van Duppen, The in-gas-jet laser ion source: resonance ionization spectroscopy of radioactive atoms in supersonic gas jets, Nucl. Instrum. Methods B 297 (2013) 7–22.
[42] R. Ferrer, A. Barzakh, B. Bastin, R. Beerwerth, M. Block, et al., Towards high-resolution laser ionization spectroscopy of the heaviest elements in supersonic gas jet expansion, Nat. Commun. 8 (2017) 14520.
[43] S.G. Johnson, B.L. Fearey, C.M. Miller, N.S. Nogar, Resonance ionization mass spectrometry of thorium: determination of the autoionization level structure and a re-determination of the ionization potential, Spectrochim. Acta B 47 (1992) 633–643.
[44] S.G. Johnson, B.L. Fearey, Spectroscopic study of thorium using continuous-wave resonance ionization mass-spectrometry with ultraviolet ionization, Spectrochim. Acta B 48 (1993) 1065–1077.
[45] Th. Billen, K. Schneider, T. Kirsten, A. Mangini, A. Eisenhauer, Resonance ionization spectroscopy of thorium, Appl. Phys. B 57 (1993) 109–112.
[46] H. Tomita, A. Nakamura, D. Matsui, R. Ohtake, V. Sonnenschein, et al., Development of two-color resonance ionization scheme for Th using an automated wide-range tunable Ti:sapphire laser system, Progr. Nucl. Sci. Technol. 5 (2018) 97–99.
[47] S. Raeder, Spurenanalyse von Aktiniden in der Umwelt mittels Resonanzionisations-Massenspektrometrie, Ph.D. thesis University of Mainz, 2010.
[48] Y. Liu, D.W. Stracener, A resonant ionization laser ion source at ORNL, Nucl. Instrum. Methods B 376 (2016) 68–72.
[49] J. Blaise, J.F. Wyart, Energy Levels and Atomic Spectra of Actinides, in International Tables of Selected Constants, Vol. 20, (Centre National de la Recherche Scientifique, Paris, France, 1992).
[50] A. Kramida, Yu. Ralchenko, J. Reader, and NIST ASD Team (2018). NIST Atomic Spectra Database (ver. 5.6.1), [Online]. Available: https://physics.nist.gov/asd [2019, May 10]. National Institute of Standards and Technology, Gaithersburg, MD. DOI: https://doi.org/10.18434/T4W30F.
[51] Y. Liu, C.U. Jost, A.J. Mendez II, D.W. Stracener, C.L. Williams, C.J. Gross, R.K. Grzywacz, M. Madurga, K. Miernik, D. Miller, et al., On-line commissioning of the HRIBF resonant ionization laser ion source, Nucl. Instrum. Methods B 298 (2013) 5.
[52] Y. Liu, J.C. Batchelder, A. Galindo-Uribarri, R. Chu, S. Fan, E. Romero-Romero, D.W. Stracener, Ion source development for ultratrace detection of uranium and thorium, Nucl. Instrum. Methods B 361 (2015) 267–272.
[53] S. Raeder, S. Fies, T. Gottwald, C. Mattolat, S. Rothe, K. Wendt, In-source resonance ionization spectroscopy of high lying energy levels in atomic uranium, Hyperfine Interact 196 (2010) 71–79.